Current Optics and Photonics
Vol. 4, No. 4, August 2020, pp. 380-390

ISSN: 2508-7266(Print) / ISSN: 2508-7274(Online)
DOI: https://doi.org/10.3807/COPP.2020.4.4.380

Reducing Efficiency Droop in (In,Ga)N/GaN Light-emitting Diodes by Improving Current Spreading with Electron-blocking Layers of the Same Size as the *n*-pad

Quoc-Hung Pham[1], Jyh-Chen Chen[1]*, and Huy-Bich Nguyen[2]

[1]*Department of Mechanical Engineering, National Central University, Jhongli City 32001, Taiwan*
[2]*Department of Mechanical Engineering, Nong Lam University, Ho Chi Minh City 700000, Vietnam*

(Received February 21, 2020 : revised May 25, 2020 : accepted June 25, 2020)

In this study, the traditional electron-blocking layer (EBL) in (In,Ga)N/GaN light-emitting diodes is replaced by a circular EBL that is the same size as the *n*-pad. The three-dimensional (3D) nonlinear Poisson, drift-diffusion, and continuity equations are adopted to simulate current transport in the LED and its characteristics. The results indicate that the local carrier-density distribution obtained for the circular EBL design is more uniform than that for the traditional EBL design. This improves the uniformity of local radiative recombination and local internal quantum efficiency (IQE) at high injection levels, which leads to a higher lumped IQE and lower efficiency droop. With the circular EBL, the lumped IQE is higher in the outer active region and lower in the active region under the *n*-pad. Since most emissions from the active region under the *n*-pad are absorbed by the *n*-pad, obviously, an LED with a circular EBL will have a higher external quantum efficiency (EQE). The results also show that this LED works at lower applied voltages.

Keywords : Light-emitting diodes, Current crowding, Efficiency droop, Electron blocking layer
OCIS codes : (230.3670) Light-emitting diodes; (160.6000) Semiconductor materials

I. INTRODUCTION

Light-emitting diodes (LEDs) have attracted much interest for solid-state lighting and display technology. However, the efficiency droop in LEDs, due to a reduction in internal quantum efficiency (IQE) that occurs at high injection levels, remains a challenge to be overcome. Efficiency droop is not caused by any single mechanism, but is related to a variety of factors that includei current crowding [1], the quantum-confined Stark effect (QCSE) [2], radiative-recombination saturation [3], Auger recombination [4], direct carrier leakage [5, 6], and leaked electrons [2]. Efficiency droop can mainly be attributed to nonradiative recombination and electron leakage inside and outside the active region. Auger recombination is an internal nonradiative processes that plays a major role in the efficiency droop in LEDs when the carrier density is high [4]. Hot carriers are generated outside of, or can be retaken by, the quantum wells (QWs) [7]. The hot-carrier effect, also known as direct carrier leakage [8], is considered to be one of the internal nonradiative processes. Here the electrons that do not completely recombine in the active layer overflow from the active region into the *p*-side layers, a process called leakage of electrons by thermionic emission. Electron leakage is also one of the most debated droop mechanisms [2]. Current crowding leads to higher carrier concentration under the *n*-pad region [9], which then causes a rise in Auger recombination and leakage of electrons in an LED, due to enhancement of local carrier densities [9, 10]. This is also a major factor in efficiency droop.

The electron-blocking layer (EBL) is a thin layer of wide-band-gap material that is inserted between the active region and the *p*-type layer. It creates a barrier to current flow in the conduction and valence bands at the active region/EBL and EBL/*p*-type interfaces. The barrier in the conduction band at the active region/EBL interface is

*Corresponding author: jcchen@ncu.edu.tw, ORCID 0000-0002-6716-0741
Color versions of one or more of the figures in this paper are available online.

capable of reducing the leakage of electrons out of the active region. Several kinds of EBLs have been developed to reduce efficiency droop in LEDs: for example, (Al,Ga)N EBLs [11], (In,Al)N EBLs [12], (In,Al)N/GaN superlattice (SL) EBLs [13], and (Al,Ga)N/GaN SL EBLs [13]. However, the barrier in the valence band at the active region/EBL interface also blocks the flow of holes to the active region, which can lead to low hole-injection efficiency [14]. As a result of polarization due to the mismatch between materials in the different layers, a positive sheet charge exists at the interface between the EBL and the active region [2], pulling down the conduction band of the EBL. This results in a reduced barrier height at the active region/EBL interface for electrons in the conduction band, while the barrier height for holes in the valence band increases. The reduced barrier height in the conduction band decreases the blocking effect of the EBL for electrons, and the increased barrier height in the valence band causes low hole-injection efficiency into the active layer, which is linked to electron leakage [14]. The blocking effect of the $Al_xGa_{1-x}N$ EBL on electrons depends on the Al composition x_{Al} [14, 15]. An increase in the Al composition of $Al_xGa_{1-x}N$ results in a wider band gap, which leads to a higher barrier at the active region/EBL interface, thereby reducing electron leakage [2] and leading to an increase in the efficiency of the LED. However, inserting an (Al,Ga)N EBL into an LED chip leads to an increase in the internal resistivity [16, 17], especially for higher Al compositions. The efficiency of the LED decreases as the Al composition in the *p*-(Al,Ga)N EBL increases [14].

The current-crowding effect, a common problem in LED structures both with and without EBLs, causes nonuniform distribution of the current density [9, 18]. Enhancement of local carrier densities leads to increased nonradiative recombination and electron leakage. Current crowding in the region under the *n*-pad of the active layer in a vertical LED structure [9] causes a faster increase in electron-current leakage in this region than in other regions; furthermore, most emissions from this region are absorbed by the *n*-pad. A more uniform current-density distribution is the key to achieving a high-efficiency LED. In a vertical LED, the EBL usually covers the entire *p*-GaN layer, although its function to counter the severe current crowding is only applicable in the region under the *n*-pad of the active layer. It is not useful for blocking electron leakage outside this region, although it does cause higher internal resistivity and lower hole-injection efficiency. A better design would allow the current to spread more easily away from the *n*-pad to the region not covered by the EBL. Less internal resistivity would lead to a more uniform distribution of current density. Such a specially designed (Al,Ga)N EBL would both improve efficiency and reduce efficiency droop in single quantum well (SQW) LEDs. LEDs with this circular EBL structure are capable of working at lower applied voltages than LEDs with the traditional EBL design. In this work, current transport is simulated using a fully three-dimensional (3D) self-consistent finite-element method (FEM) developed with COMSOL Multiphysics. The 3D numerical model used to investigate the current transport is calculated by solving the continuity equation and the drift-diffusion equation, along with the Poisson equation. Fermi-Dirac statistics are applied to solve the Poisson, drift-diffusion, and continuity equations. The lumped IQE of an LED with the standard (Al,Ga)N EBL is compared to experimental results [19].

II. PHYSICAL MODELING AND NUMERICAL METHOD

Figures 1(a) and 1(b) show the structure of a vertical (In,Ga)N/GaN SQW LED design with a 0.003-μm-thick $Al_{0.1}Ga_{0.9}N$ EBL sandwiched between the 0.0023-μm-thick active region and the 0.18-μm-thick *p*-type GaN layer, 212×212 μm^2 in area (structure 1, (S1)) [19, 20]. The *p*-pad, *n*-pad and *n*-GaN layer are 0.01 μm, 0.01 μm, and 5 μm thick respectively. The active region includes two GaN barrier layers with one (In,Ga)N active layer. The $In_{0.19}Ga_{0.81}N$ active layer and GaN barrier layer are 3 nm and 10 nm thick respectively. A 40-μm-radius circular *n*-pad is formed on the top *n*-GaN surface [20]. As can be seen in Figs. 1(c) and 1(d), the square shape of the EBL in Fig. 1(a) is changed to a circular $Al_{0.1}Ga_{0.9}N$ EBL (structure 2 (S2)), only in the region under the *n*-pad; the diameter is the same as that of the *n*-pad layer. The doping profiles of the *n*-GaN, EBL, and *p*-GaN layer are 2×10^{18} cm^{-3}, 6×10^{17} cm^{-3}, and 2×10^{18} cm^{-3} respectively. The active-region layers are undoped. The thickness of the *p*-GaN is 0.183 μm. The doping profiles of the *p*-GaN, EBL, and *n*-GaN are 2×10^{18} cm^{-3}, 2×10^{18} cm^{-3}, and 6×10^{17} cm^{-3} respectively. In this study, the EBL's Al composition in S1 and S2 varies from 0.05 to 0.14.

The Poisson, drift-diffusion, and continuity equations [9, 10] are

$$\nabla^2 V = \left(n - p + N_A^- - N_D^+\right)/\varepsilon, \tag{1}$$

$$J_n = -\mu_n n \nabla V + q D_n \nabla n, \tag{2}$$

$$J_p = -\mu_p p \nabla V + q D_p \nabla p, \tag{3}$$

$$\nabla \cdot J_{n,p} = R_{SRH} + R_{rad} + R_{Auger} + R_{lk}, \tag{4}$$

where ε is the permittivity of a dielectric material; V is the electrostatic potential; n is the electron concentration and p is the hole concentration; N_A^- represents the concentration of ionized acceptors and N_D^+ the concentration of ionized donors; J_n and J_p are the carrier current densities of electrons and holes respectively; μ_n and μ_p are the electron and hole mobilities respectively; R_{srh} is the rate of

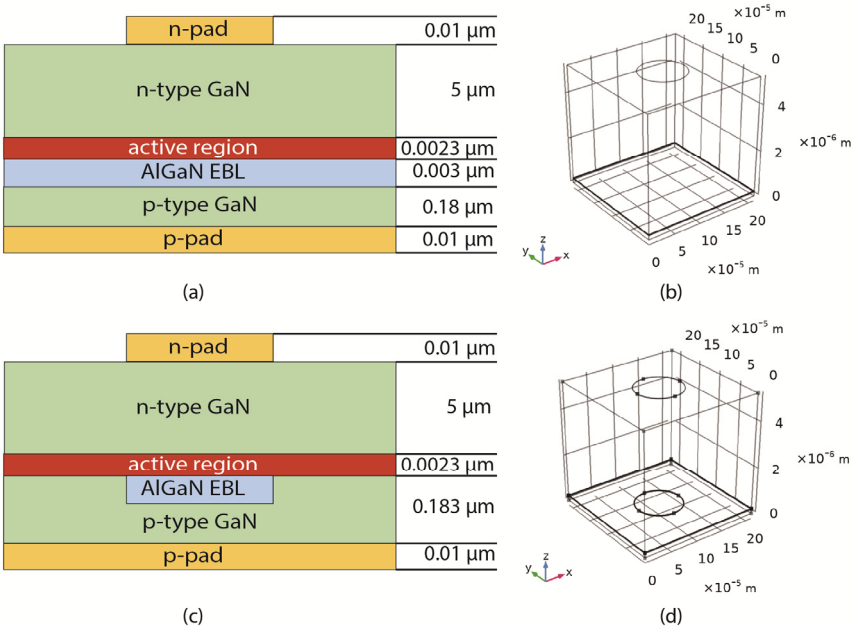

FIG. 1. Schematic diagrams of vertical SQW LEDs with (a, b) a traditional EBL and (c, d) a specially designed EBL: (a) and (c) show the layer compositions, while (b) and (d) present the 3D structures.

Shockley-Read-Hall (SRH) recombination; R_{rad} is the rate of radiative recombination; R_{Auger} is the rate of Auger recombination; and R_{lk} is the total rate of carrier leakage, which includes direct carrier and electron leakage. In this study, the carrier mobilities were obtained using Arora mobility model [21]. The leakage of holes generated by thermionic emission is neglected, due to the lower hole mobility compared to electron mobility in the highly doped *p*-GaN. The recombination rates for both electrons and holes are assumed to be the same in this study. The band offset ratio between GaN and $Al_xGa_{1-x}N$ is 0.5, the same as in previous studies [2, 17, 22]. Deformation of the QWs is caused by polarization [2]; the total polarization includes both spontaneous and piezoelectric components. The model developed by Fiorentini *et al.* [23] is employed to include the polarization effect in the internal LED interfaces, which is a function of the compositions and lattice constants of the materials. The alloy lattice constant is calculated by Vegard's Law. Polarization leads to a surface charge [23] at the interfaces between different materials, defined as follows:

$$\begin{aligned}\sigma_p\left(P_{sp}+P_{pz}\right) &= P(bottom)-P(top)\\ &=\left[P_{sp}(bottom)+P_{pz}(\text{bottom})\right]\\ &-\left[P_{sp}(top)+P_{pz}(top)\right],\end{aligned} \tag{5}$$

where σ_p is the surface charge P_{sp} and P_{pz} are the spontaneous and piezoelectric polarizations respectively. However, the value of the surface charge found in the experiments in [24] is a factor of 0.2 to 0.8 smaller than the value calculated by Eq. (5). In theoretical and simulation studies, the surface charge calculated by Eq. (5) is usually scaled down by a fit factor; here the fit factor is selected to be 0.4, the same as in our previous study [24]. The surface charge only appears at the interfaces between the QW/GaN barrier layer, GaN barrier layer/EBL, and EBL/*p*-GaN layer interfaces in this study. At the interfaces of different materials, the condition $(D_1-D_2)\cdot\hat{n}=\sigma_p$ is applied for the displacement D of the electric field [25], where the subscript represents the layer.

The rate of Shockley-Read-Hall (SRH) recombination R_{SRH} [9] is given by

$$R_{SRH}=(pn-n_i^2)\Big/\left(\tau_n\left[p+n_te^{(E_t-E_i)/k_BT}\right]+\tau_p\left[n+n_te^{(E_t-E_i)/k_BT}\right]\right), \tag{6}$$

where k_B is Boltzmann's constant; T is the temperature of the lattice; E_t is the trap energy; and E_i and n_i are the Fermi level and carrier density in the intrinsic semiconductor. τ_n is the SRH recombination coefficient for electrons and τ_p is the SRH recombination coefficient for holes. The SRH carrier lifetime, including the PSF effect, developed in our previous study [10] is given by

$$\tau_{SRH}=\tau_{p0}\frac{1}{1+(p/n_0)}+\frac{\tau_{n0}}{1+(N_0/n)^{\gamma}}\frac{1}{1+(n/n_0)}, \tag{7}$$

where n_0 represents the PSF-effect coefficient. The chosen background electron density N_0 is 1×10^{17} cm^{-3}, and a dimensionless exponent $\gamma=0.4$ is chosen to match the simulation result to the experimentally measured IQE. The

PSF coefficient is set to be 1×10^{19} cm^{-3}, so that the simulation results match the experimentally measured IQE [26-28]. The term γ is used to deal with the uncertainty arising from the defect structure of crystals and material impurities. The experimental carrier lifetime at very low injection levels is from 1×10^{-6} to 5×10^{-9} s [8, 29-32]. Here $\tau_{p0} = 0.1 \times 10^{-7} s$ is chosen, as found in an LED that has the same thickness and In mole fraction of the well layer [33], while $\tau_{n0} = 0.15 \times 10^{-7}$ s is chosen to correspond to the experimentally measured IQE.

The rate of radiative recombination [34] is given by

$$R_{Rad} = B(np - n_i^2), \tag{8}$$

where B is the radiative coefficient. The radiative coefficient, based on electron density and the PSF effect [10, 35], is given by

$$B = B_0 / \left(1 + \left(np / \mathrm{n}_0^2\right)\right), \tag{9}$$

where B_0, including the PSF effect coefficient n_0, is the radiative recombination coefficient at extremely low injection levels. A B value is chosen from 1×10^{-11} to 1.5×10^{-9} cm^3 s^{-1} [36, 37]; $B_0 = 2.21 \times 10^{-10}$ cm^3 s^{-1} is used in this study, to match the experimental IQE characteristics.

The Auger recombination rate [38] is given by

$$R_{Auger} = C_n(n^2 p - n_i^2) + C_p(np^2 - n_i^2), \tag{10}$$

where C_n and C_p represent the Auger coefficients for holes and electrons respectively. The Auger coefficient [35] is given by $C_n = C_{n0} / \left(1 + \left(n / \mathrm{n}_0\right)\right)$ and $C_p = C_{p0} / \left(1 + \left(p / \mathrm{n}_0\right)\right)$, where C_0, including the PSF effect coefficient n_0, is the coefficient at very low injection levels. The value of $C_{n,p}$ is in the range of 1.4×10^{-30} to 3.5×10^{-34} cm^6 s^{-1} [27, 31, 39]. The selected values of parameters C_{n0} and C_{p0} are 8×10^{-31} cm^6 s^{-1} in this study, to match the experimental IQE characteristics. The direct leaked carrier rate assisted by Auger recombination can be described by $R_{lk,n}^{Auger} = C_{lk,n}(n^2 p - n_i^2)$ and $R_{lk,p}^{Auger} = C_{lk,p}(np^2 - \mathrm{n}_i^2)$, [40] for electrons and holes respectively. The direct leaked carrier coefficients can be described by $C_{lk,n} = l^2 C_n$ and $C_{lk,p} = l^2 C_p$. A dimensionless $l = 3$ is chosen to match the experimentally measured IQE [40]. Other carriers leak by thermionic emission, where $R_{lk,n}^{th}$ indicates the leaked electrons and $R_{lk,p}^{th}$ the leaked holes.

The local IQE, $\mathrm{IQE}_{\mathrm{local}}$, can be described by

$$IQE_{local} = R_r / (\mathrm{R}_r + R_{SRH} + R_{Au} + R_{lk}). \tag{11}$$

The recombination currents are calculated by integrating the recombination distribution rates over the whole active layer. The lumped $\mathrm{IQE}_{\mathrm{lumped}}$ can be described by

$$IQE_{lumped} = I_r / (I_{total}), \tag{12}$$

where I_r and $\mathrm{I}_{\mathrm{total}}$ are the total radiative recombination current and total injection current respectively.

The finite-element method (FEM) used to solve the 3D Poisson, drift-diffusion, and continuity equations was developed using the COMSOL Multiphysics software. The numerical scheme has already been described in detail in our previous work [10]. The number of elements used in the convergence testing for both S1 and S2 are 92,400, 141,000, and 298,800. The simulation result for the 141,000 case is almost the same as that for the 298,800 case. To save on computer memory and shorten computation time, the 141,000-element example is chosen for both LED structures. A relative tolerance of 1×10^{-5} is chosen for the electrostatic potential and carrier concentration.

III. RESULTS AND DISCUSSION

The average injection-current density is defined as the ratio of the injection current to the cross-sectional area of the active layer. Figure 2 shows the energy-band diagrams for S1 and S2, at the central and outer positions of the chip, for two different injection-current densities. At 0.1 A/cm^2, there is little carrier drift with the application of the electric field. Carrier flow through the chip is mainly due to diffusion; carriers must climb over a potential hill to cross to the other side (Fig. 2(a)). The band bending at the GaN barrier/QW, active region/EBL and EBL/*p*-GaN interfaces appears due to the polarization charge, which is similar to the mechanism predicted in previous studies [36, 41]. This also causes reduction of the barrier height at the GaN barrier/EBL interface for electrons in the conduction band, which is similar to the mechanism predicted in a previous study [42]. The reduction in the barrier height in the conduction band decreases the blocking effect of the EBL; the EBL makes the potential hill higher. For S1 there is not much difference in the energy band between the central and outer positions, so Fig. 2(a) only shows the energy band for the center. For S2 the potential hill between the active region and the p-GaN is lower at the outer position, due to the absence of the EBL. As a consequence, carriers need less energy to flow through the outer region compared to the center.

The barrier height in the conduction band at the *n*-GaN layer/GaN barrier layer interface is lower at the outer position in S2 than in S1, so the electrons in S2 need less energy to cross the barrier and flow into the QW. On the other hand, in S1 more energy is needed for the holes to climb the higher barrier in the valence band at the EBL/GaN barrier layer than in S2. At 120 A/cm^2 there is greater carrier drift caused by the applied electric field, and the flow of carriers through the chip is driven by both drift and diffusion processes. The stronger applied electric

field at the center in comparison to the outer region [43] leads to a stronger carrier flow, which results in current crowding in the central region. Moreover, the higher applied electric field at the center also causes the energy-band level in the n-GaN to be higher here than in the outer position, while the energy-band level of the p-GaN is almost the same for both positions (Fig. 2(b)). The potential hill is not as steep as in the case for 0.1 A/cm^2. The energy-band diagrams for S1 and S2 are quite similar at the center, due to the presence of the EBL in both structures. The barrier height of the conduction band at the GaN barrier/*n*-GaN interface is higher in S2 than in S1, so electrons need more energy to cross the barrier and flow into the QW. The barrier height of the valence band at the EBL/GaN barrier layer interface is almost the same in both structures. In S1 the energy-band level of *n*-GaN is higher in the outer location compared to that in S2, due to the higher applied electric field. The valence band at the active region/EBL interface in S1 acts as a barrier, which does not exist in S2. Therefore, it is easier for holes to flow into the active layer from the *p*-GaN in S2, leading to the higher hole concentration in the outer region, in comparison to S1.

The electron current-density distribution at the center of the *yz* plane of the LED chip, at various injection levels from 0.1 to 120 A/cm^2, for S1 and S2 is shown in Fig. 3. The shaded region represents the region under the *n*-pad in

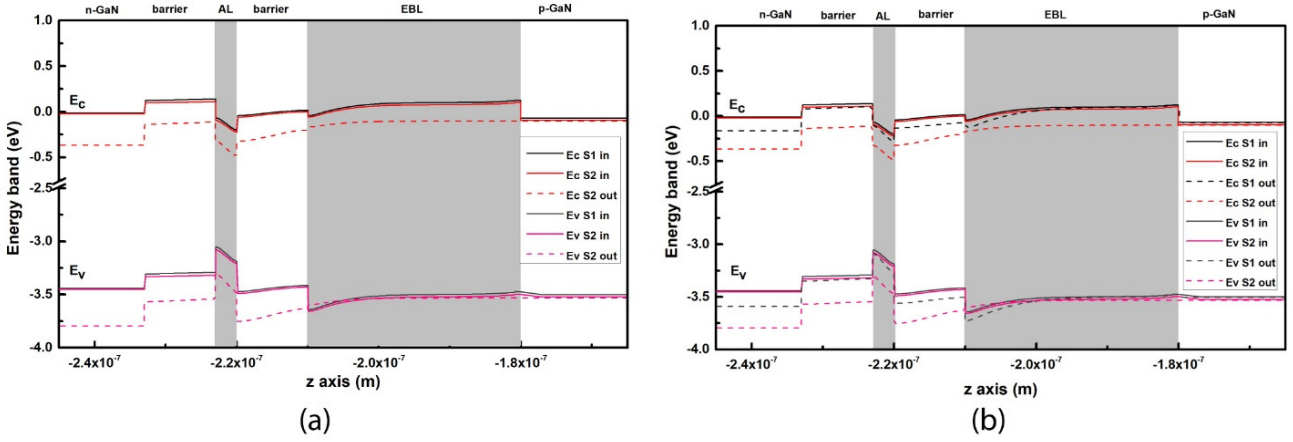

FIG. 2. Energy-band diagrams for S1 and S2, for (a) 0.1 A/cm^2 and (b) 120 A/cm^2, at the center and the outer position ($x = 5 \times 10^{-5}$ m and $y = 5 \times 10^{-5}$ m) of the chip. E_c and E_v represent the conduction band and valence band respectively; "in" and "ou" represent the energy band at the center and outer positions respectively.

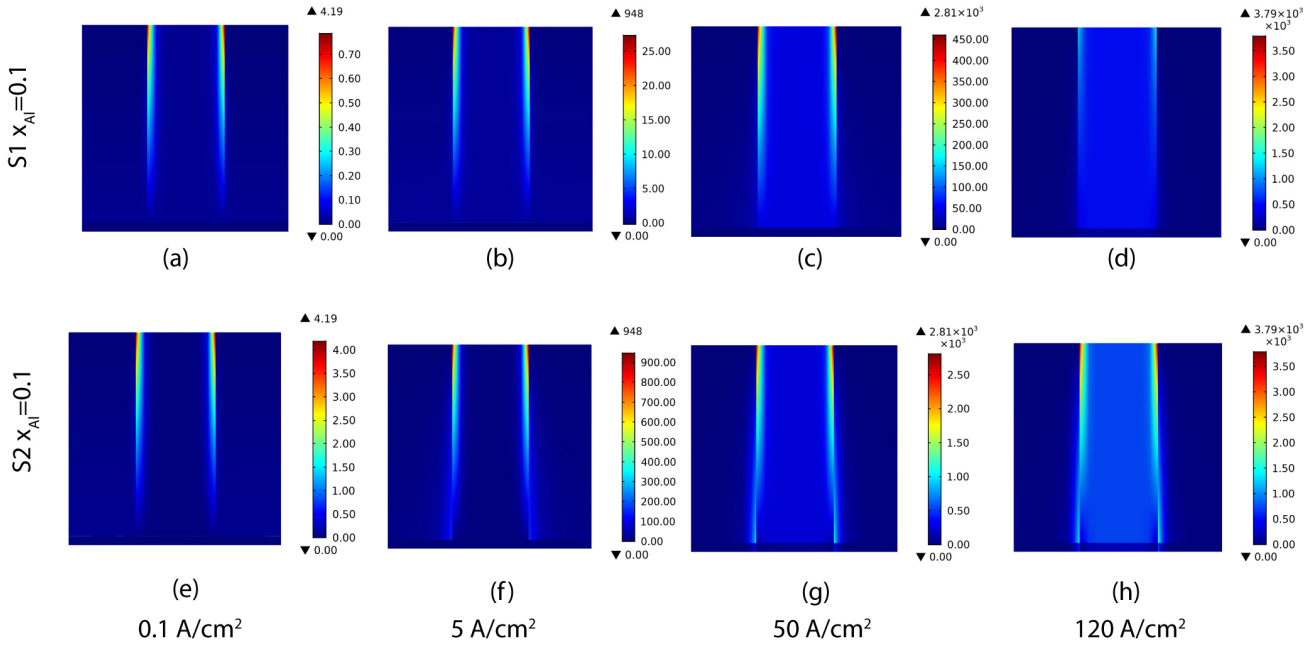

FIG. 3. Electron current density (in A/cm^2) at the center of the *yz* plane of the chip, at various injection-current densities: (a), (b), (c), and (d) for S1, and (e), (f), (g), and (h) for S2.

the active layer. The distribution of the electron current density shows crowding near the *n*-pad, at all injection levels. With rising injection level, the difference in carrier current density between the shaded region and the outer region becomes more significant. At high injection levels there is current crowding in and near the shaded region, due to the stronger carrier flow driven by a stronger applied electric field in this region. The maximum electron current density, which occurs near the edge of the *n*-pad, is due to the singular electric field at the interface between the metal and semiconductor layers [44]. For 0.1 A/cm^2 (Figs. 3(a) and 3(e)), the distributions of the electron current density are quite similar in both structures, due to the energy-band level of *n*-GaN being the same (Fig. 2(a)). Few electrons have enough energy to cross the QW at this level of injection current, because of the high potential hill (Fig. 2(a)), and the effect of the EBL on the electrons is insignificant at low injection levels. At 5 A/cm^2 the electron current density is slightly lower in the outer region of S1, compared to the region under the *n*-pad (Fig. 3(b)). On the other hand, for S2 the crowding effect is not very significant (Fig. 3(b)), due to the absence of EBL in the outer region. For higher injection currents (Figs. 3(c) and 3(d)), the crowding effect becomes more serious under the *n*-pad region, for S1. For S2, the crowding becomes significant (Figs. 3(g) and 3(h)) but is less severe than in the S1 case. This is expected, since the energy band of the *n*-GaN in the shaded region is higher in S1 than in S2 (Fig. 2(b)).

Figures 4(a) and 4(b) show the distributions of the electron and hole concentrations along the *x* axis of the active layer for the various injection levels, for S1 and S2 respectively. Here the carrierdensity distributions in the active layer are nonuniform at all injection-current densities; the degree of nonuniformity worsens as the injection current becomes higher. In S1 the electron concentration in the shaded region is always higher than in the outer region, regardless of the injection current, due to the stronger applied electric field, while this trend is reversed in S2.

In S2 the electron concentration is lower in the shaded region at lower injection-current densities, due to the higher barrier in the conduction band at the *n*-GaN layer/GaN barrier layer interface, and the higher potential hill generated by the circular EBL (Fig. 2(a)). At higher injection levels this concentration becomes higher, because of the crowding effect caused by the stronger applied electric field. The hole concentration under the *n*-pad is also always higher in S1, due to the stronger applied electric field in this region. In S2, the hole concentration is higher in the outer region at lower injection levels due to the lower potential hill without the EBL in this region (Fig. 2(a)), making it easier for holes to flow into the active layer from the *p*-GaN. At higher injection levels the trend is reversed, due to the stronger crowding in the shaded region. The hole concentration in the outer location is lower in S1 than that in S2 at all injection levels, since the barrier generated by the EBL does not exist in the outer region for S2 (Fig. 2). From Figs. 4(a) and 4(b), we can see that the circular EBL in S2 is capable of mitigating the crowding effect in the shaded region at high injection levels.

The local radiative recombination in the active layer at various injection levels for S1 and S2 is shown in Fig. 5(a). There is a nonuniform distribution of radiative recombination in the active layer at all injection levels, due to the current crowding effect, increasing in magnitude as the injection level increases. In S1 the radiative recombination is always higher in the shaded region than in the outer region, regardless of the injection level, as expected from the carrier-concentration distribution (Figs. 4(a) and 4(b)). In S2, at low injection current the radiative recombination is lower in the shaded region than in the outer region, due to the effect of the circular EBL. At high injection-current densities the trend is reversed, due to the higher carrier density in this region (Figs. 4(a) and 4(b)).

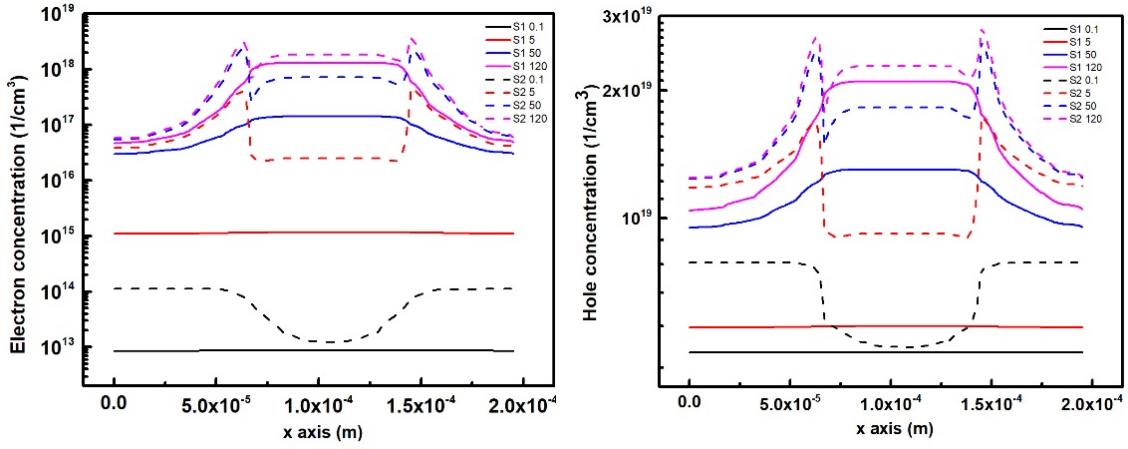

FIG. 4. Local carrier concentration along the *x* axis ($y = 1.06 \times 10^{-4}$ m) in the active layer of the LED chip, for various injection levels: (a) electron concentration and (b) hole concentration.

Figure 5(b) shows the local electron density in the *p*-GaN, or electron leakage from the active region, at various injection-current densities, for S1 and S2. The local electron-density distributions in the *p*-GaN layer are not uniform for all injection-current densities, due to the crowding effect, which increases in magnitude as the injection current rises. Electron leakage in the outer region is much lower in S2 than in S1. It is obvious that the leakage of electrons has been significantly reduced by using a circular EBL (as in S2), rather than a traditional EBL (as in S1).

Figure 6 shows the lumped recombination-current density arising from the recombination processes in both the shaded and outer regions, for various injection current levels, for S1 and S2. When the injection level increases, the lumped SRH recombination-current density starts to rise sooner than the other recombination processes, due to its lower-order dependence on carrier density than those for the other processes, after which the densities for radiative, Auger, direct carrier-leakage recombination, and leaked electrons begin to increase in turn. Figs. 6(a) and 6(b) show the results for the lumped recombination-current density for the shaded region in both structures, which is lower than that in the outer region, at low injection currents. At higher injection levels the trend is reversed, because the applied electric field is higher in the shaded region than in the outer region, leading to an increase in carrier density in this region (Figs. 4(a) and 4(b)). In the shaded region (Fig. 6(a)), all recombination processes occur earlier in S1 and are higher in magnitude, compared to S2. In the outer region (Fig. 6(b)), there is no significant difference in the recombination processes between S1 and S2, at low injection current densities. At high injection current densities, however, the magnitude of each recombination

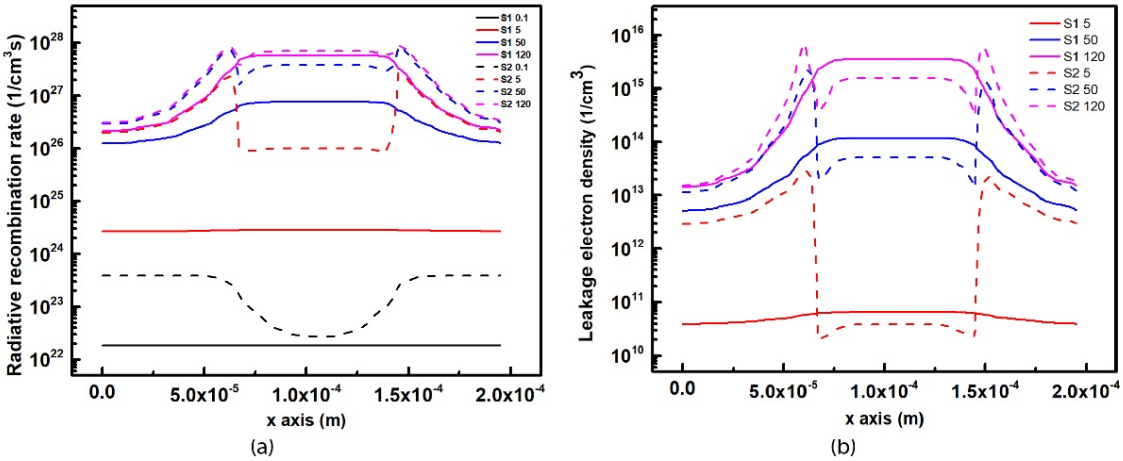

FIG. 5. (a) Radiative recombination along the x axis ($y = 1.06 \times 10^{-4}$ m) of the active layer and (b) leakage of electron density along the x axis ($y = 1.06 \times 10^{-4}$ m) in the *p*-GaN of the LED chip, for various injection levels.

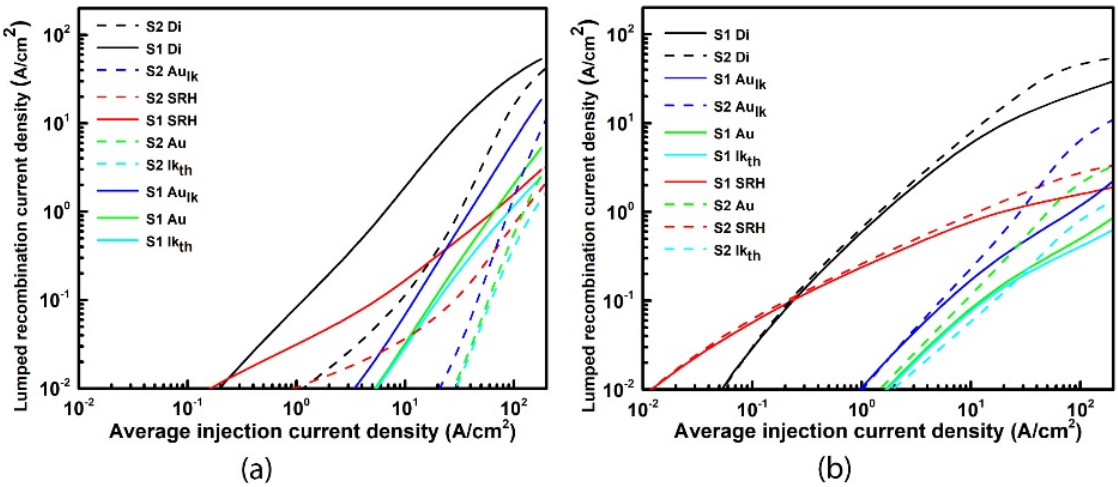

FIG. 6. Lumped recombination-current density versus average injection-current density, for S1 and S2, in the (a) shaded and (b) outer regions. "Di", "SRH", "Au", "Au$_{lk}$", and "lk$_{th}$" respectively represent the lumped radiative, SRH, Auger, and direct leakage recombination-current density and electrons leaked by thermionic emission.

process is higher in S2 than in S1, due to the higher hole density (Fig. 4(a)).

Figure 7 shows the local IQE in the active layer for the various injection levels, for S1 and S2. The distributions of the local IQE are nonuniform. In S1 there is an inversion in the magnitude of the local IQE from higher to lower, when the injection level rises. The reason for this is saturation of the radiative-recombination current and the fast rise of nonradiative recombination in the shaded region, as shown in Fig. 7(a). In S2, at low injection levels the local IQE is higher in the outer region rather than in the shaded region, as expected from the radiative-recombination distribution (Fig. 6); at higher injection levels the trend is reversed, as expected from radiative recombination (Fig. 6). At this injection level more carriers accumulate in the shaded region compared to the outer region, due to the crowding effect, which leads to higher radiative-recombination results in the higher local IQE in this region. The local IQE distribution is less uniform in S1 than in S2. Obviously the circular EBL can elevate the IQE in the outer region and mitigate current crowding in the shaded region, which will be of great benefit to LED performance.

The total lumped IQE in the active layer versus average injection-current density is shown in Fig. 8. Lumped IQE versus average injection-current density in the shaded region, the outer region, and the entire region of the active layer, for S1 and S2, are shown in Fig. 8(a). Galler *et al.* [19] calculated the IQE from experimental measurements of the external quantum efficiency (EQE) and the extraction efficiency η_{extr} through IQE = EQE/η_{extr}. The absorption effect from the various layers in the LED, especially from the *n*-pad, is included in η_{extr}. Both experiment and simulation show that the lumped IQEs rise quickly and then drop significantly after reaching their peak values. The peak value is higher in S2 than in S1, and occurs at a higher injection level. It is obvious that the efficiency droop can be mitigated by using a circular EBL (S2) instead of a traditional EBL structure (S1). The lumped IQE begins to rise earlier in the outer region in S2 and is higher in magnitude compared to that in S1, due to the higher lumped radiative recombination (Figs. 6(b) and 7). The peak value of lumped IQE in the outer region is much higher in S2.

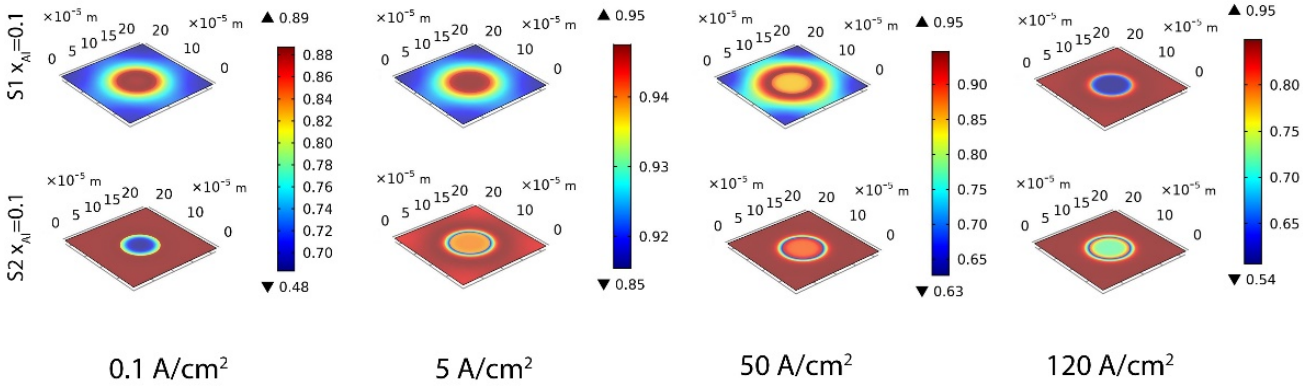

FIG. 7. Local distribution of IQE in the active layer for various injection levels. The top row is for S1, and the bottom row is for S2.

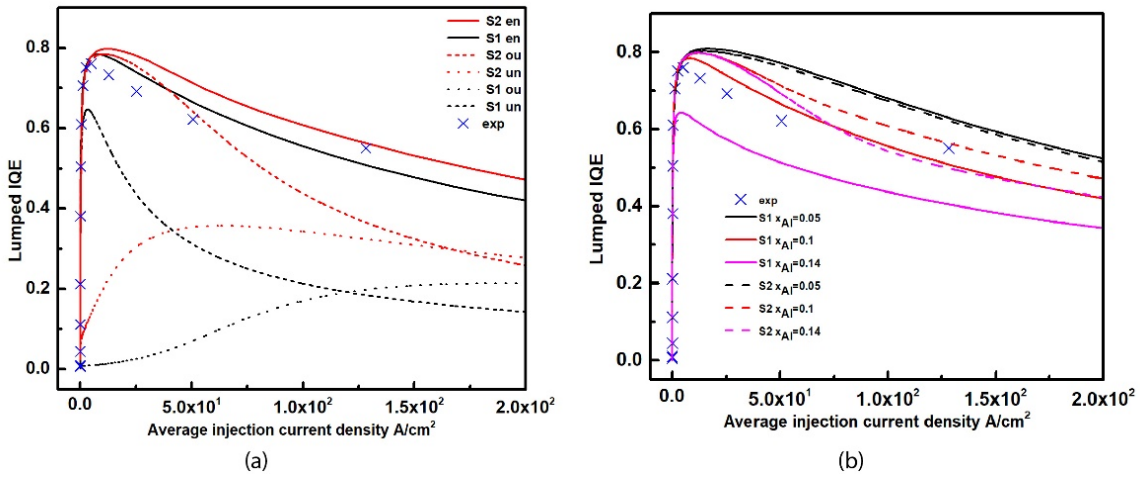

FIG. 8. (a) Lumped IQE versus average injection-current density in S1 and S2, in the shaded region (un), the outer region (ou), and the entire region (en) of the active layer. (b) Lumped IQE versus average injection-current density in S1 and S2, for various EBL Al compositions. Here "×" represents the experimental results of reference [19].

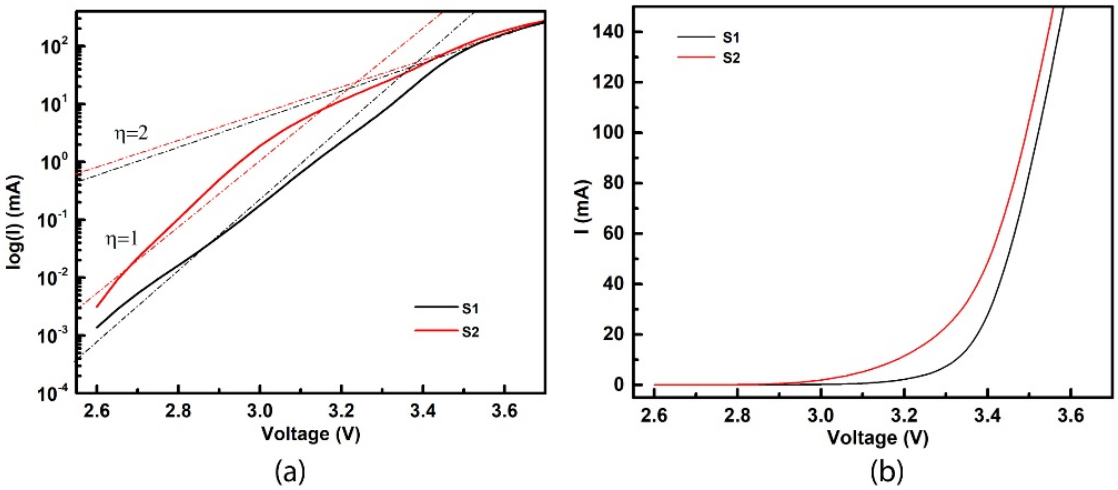

FIG. 9. Computed current-voltage characteristics in (a) logarithmic scale and (b) linear scale for the two structures. η is the ideality factor.

In S1, the lumped IQE in the outer region reaches its peak at 2 A/cm^2, while it peaks around 8 A/cm^2 in S2. In the shaded region most of the photons generated from radiative recombination in the active layer are absorbed by the *n*-pad, which leads to a reduction of EQE in the LEDs. The lumped IQE is much higher in the shaded region in S1 compared to S2, at all injection levels. It is obvious that an LED chip with a circular EBL will have a higher EQE than one with a traditional EBL.

The lumped IQE versus average injection-current density in S1 and S2 for various EBL Al compositions is shown in Fig. 8(b). The peak value of the lumped IQE is higher when the Al composition of the EBL is lower, which is consistent with previous simulation results [17]. The injection current needed to reach peak IQE is lower when the Al composition of the EBL is higher. The lumped IQE is more significantly affected by the Al composition of the EBL in structure 1 than in structure 2. In other words, the effect of increasing Al composition of the EBL on the lumped IQE is less significant in structure 2 than in structure 1.

The current-voltage (*I-V*) curves for S1 and S2 are shown in Fig. 9. The current-voltage characteristics for S1 and S2, plotted using a logarithmic scale, are shown in Fig. 9(a), and using a linear scale in Fig. 9(b). The LEDs turn on at around 2.9 V for S1 and 2.8 V for S2. An increase of the injection current results in an increase of the voltage drop. The LED moves from a low-injection region to a high-injection region, where the ideality factor η changes from 1 to 2, at about 3.2 V in S2 and 3.4 V in S1.

IV. CONCLUSION

In this study, the traditional square EBL is replaced with a circular EBL to improve the efficiency of an LED chip. The distribution of the local carrier concentration in the structure with the circular EBL is more uniform than that in the structure with the traditional EBL, leading to a more uniform distribution of radiative recombination and of local IQE at high injection-current density. The results show that one can obtain reduced efficiency droop by replacing the traditional EBL with a circular one. The lumped IQE in the outer active region is higher for the circular EBL than for the traditional EBL. There is a significant increase in lumped IQE in the shaded region for the traditional EBL as the injection level rises, which is the major contribution to the IQE for the entire chip at higher injection levels. On the other hand, lumped IQE is much lower in the shaded region in S2 than in S1, at all injection levels; emission from the shaded region may be absorbed by the *n*-pad, which causes a decrease in EQE. The lumped IQE in the shaded region is lower in the structure with the circular EBL than the one with the traditional structure. It is clear that EQE can be enhanced by replacing the traditional EBL with a circular structure. The LED with a circular EBL works at a lower applied voltage, and the effect of Al composition of the EBL on the efficiency is greater for structure 1 than for structure 2.

ACKNOWLEDGMENT

The authors gratefully acknowledge the financial support of the Ministry of Science and Technology of Taiwan (MOST), R.O.C. for this work, through Grant No. MOST 104-2221-E-008-079-MY3.

REFERENCES

1. X. Guo and E. F. Schubert, "Current crowding in GaN/InGaN light emitting diodes on insulating substrates," J. Appl. Phys. **90**, 4191-4195 (2001).

2. M.-H. Kim, M. F. Schubert, Q. Dai, J. K. Kim, E. F. Schubert, J. Piprek, and Y. Park, "Origin of efficiency droop in GaN-based light-emitting diodes," Appl. Phys. Lett. **91**, 183507 (2007).
3. D.-S. Shin, D.-P. Han, J.-Y. Oh, and J.-I. Shim, "Study of droop phenomena in InGaN-based blue and green light-emitting diodes by temperature-dependent electroluminescence," Appl. Phys. Lett. **100**, 153506 (2012).
4. Y. C. Shen, G. O. Mueller, S. Watanabe, N. F. Gardner, A. Munkholm, and M. R. Krames, "Auger recombination in InGaN measured by photoluminescence," Appl. Phys. Lett. **91**, 141101 (2007).
5. M. Binder, A. Nirschl, R. Zeisel, T. Hager, H.-J. Lugauer, M. Sabathil, D. Bougeard, J. Wagner, and B. Galler, "Identification of *nnp* and *npp* Auger recombination as significant contributor to the efficiency droop in (GaIn)N quantum wells by visualization of hot carriers in photoluminescence," Appl. Phys. Lett. **103**, 071108 (2013).
6. E. Kioupakis, P. Rinke, K. T. Delaney, and C. G. Van de Walle, "Indirect Auger recombination as a cause of efficiency droop in nitride light-emitting diodes," Appl. Phys. Lett. **98**, 161107 (2011).
7. K. D. Chik, "A theoretical analysis of Auger recombination induced energetic carrier leakage in GaInAsP/InP double heterojunction lasers and light emitting diodes," J. Appl. Phys. **63**, 4688-4698 (1988).
8. A. Laubsch, M. Sabathil, W. Bergbauer, M. Strassburg, H. Lugauer, M. Peter, S. Lutgen, N. Linder, K. Streubel, J. Hader, J. V. Moloney, B. Pasenow, and S. W. Koch, "On the origin of IQE-'droop' in InGaN LEDs," Phys. Status Solidi C **6**, S913-S916 (2009).
9. C.-K. Li and Y.-R. Wu, "Study on the current spreading effect and light extraction enhancement of vertical GaN/InGaN LEDs," IEEE Trans. Electron Devices **59**, 400-407 (2012).
10. Q.-H. Pham, J.-C. Chen, and H.-B. Nguyen, "Three-dimensional numerical study on the efficiency droop in InGaN/GaN light-emitting diodes," IEEE Photon. J. **11**, 1-17 (2019).
11. L. Zhang, X. C. Wei, N. X. Liu, H. Lu, J. P. Zeng, J. X. Wang, Y. P. Zeng, and J. M. Li, "Improvement of efficiency of GaN-based polarization-doped light-emitting diodes grown by metalorganic chemical vapor deposition," Appl. Phys. Lett. **98**, 241111 (2011).
12. S. Choi, H. J. Kim, S.-S. Kim, J. Liu, J. Kim, J.-H. Ryou, R. D. Dupuis, A. M. Fischer, and F. A. Ponce, "Improvement of peak quantum efficiency and efficiency droop in III-nitride visible light-emitting diodes with an InAlN electron-blocking layer," Appl. Phys. Lett. **96**, 221105 (2010).
13. Y.-Y. Zhang, X.-L. Zhu, Y.-A. Yin, and J. Ma, "Performance enhancement of near-UV light-emitting diodes with an InAlN/GaN superlattice electron-blocking layer," IEEE Electron Device Lett. **33**, 994-996 (2012).
14. S.-H. Han, D.-Y. Lee, S.-J. Lee, C.-Y. Cho, M.-K. Kwon, S. P. Lee, D. Y. Noh, D.-J. Kim, Y. C. Kim, and S.-J. Park, "Effect of electron blocking layer on efficiency droop in InGaN/GaN multiple quantum well light-emitting diodes," Appl. Phys. Lett. **94**, 231123 (2009).
15. K.-H. Kim, S.-W. Lee, S.-N. Lee, and J. Kim, "Effect of p-$Al_xGa_{1-x}N$ electron blocking layer on optical and electrical properties in GaN-based light emitting diodes," J. Vac. Sci. Technol. B: Nanotechnol. Microelectron.: Mater., Process., Meas., Phenom. **30**, 061204 (2012).
16. L. Zhang, K. Ding, N. X. Liu, T. B. Wei, X. L. Ji, P. Ma, J. C. Yan, J. X. Wang, Y. P. Zeng, and J. M. Li, "Theoretical study of polarization-doped GaN-based light-emitting diodes," Appl. Phys. Lett. **98**, 101110 (2011).
17. C. S. Xia, Z. M. Simon Li, and Y. Sheng, "On the importance of AlGaN electron blocking layer design for GaN-based light-emitting diodes," Appl. Phys. Lett. **103**, 233505 (2013).
18. S. H. Tu, J. C. Chen, F. S. Hwu, G. J. Sheu, F. L. Lin, S. Y. Kuo, J. Y. Chang, and C. C. Lee, "Characteristics of current distribution by designed electrode patterns for high power ThinGaN LED," Solid-State Electron. **54**, 1438-1443 (2010).
19. B. Galler, P. Drechsel, R. Monnard, P. Rode, P. Stauss, S. Froehlich, W. Bergbauer, M. Binder, M. Sabathil, and B. Hahn, "Influence of indium content and temperature on Auger-like recombination in InGaN quantum wells grown on (111) silicon substrates," Appl. Phys. Lett. **101**, 131111 (2012).
20. B. Hahn, B. Galler, and K. Engl, "Development of high-efficiency and high-power vertical light emitting diodes," Jpn. J. Appl. Phys. **53**, 100208 (2014).
21. N. D. Arora, J. R. Hauser, and D. J. Roulston, "Electron and hole mobilities in silicon as a function of concentration and temperature," IEEE Trans. Electron Devices **29**, 292-295 (1982).
22. J. Piprek and S. Li, "Electron leakage effects on GaN-based light-emitting diodes," Opt. Quantum Electron. **42**, 89-95 (2010).
23. V. Fiorentini, F. Bernardini, and O. Ambacher, "Evidence for nonlinear macroscopic polarization in III-V nitride alloy heterostructures," Appl. Phys. Lett. **80**, 1204-1206 (2002).
24. J.-R. Chen, C.-H. Lee, T.-S. Ko, Y.-A. Chang, T.-C. Lu, H.-C. Kuo, Y.-K. Kuo, and S.-C. Wang, "Effects of built-in polarization and carrier overflow on InGaN quantum-well lasers with electronic blocking layers," J. Lightwave Technol. **26**, 329-337 (2008).
25. D. J. Griffiths, "Introduction to electrodynamics," Am. J. Phs. **73**, 574 (2005).
26. P. Tian, J. J. D. McKendry, J. Herrnsdorf, S. Watson, R. Ferreira, I. M. Watson, E. Gu, A. E. Kelly, and M. D. Dawson, "Temperature-dependent efficiency droop of blue InGaN micro-light emitting diodes," Appl. Phys. Lett. **105**, 171107 (2014).
27. E. Kioupakis, Q. Yan, D. Steiauf, and C. G. Van de Walle, "Temperature and carrier-density dependence of Auger and radiative recombination in nitride optoelectronic devices," New J. Phys. **15**, 125006 (2013).
28. H. Fu, Z. Lu, and Y. Zhao, "Analysis of low efficiency droop of semipolar InGaN quantum well light-emitting diodes by modified rate equation with weak phase-space filling effect," AIP Advances **6**, 065013 (2016).
29. H.-Y. Ryu, D.-S. Shin, and J.-I. Shim, "Analysis of efficiency droop in nitride light-emitting diodes by the reduced effective volume of InGaN active material," Appl. Phys. Lett. **100**, 131109 (2012).
30. Q. Dai, M. F. Schubert, M. H. Kim, J. K. Kim, E. F. Schubert, D. D. Koleske, M. H. Crawford, S. R. Lee, A. J.

Fischer, G. Thaler, and M. A. Banas, "Internal quantum efficiency and nonradiative recombination coefficient of GaInN/GaN multiple quantum wells with different dislocation densities," Appl. Phys. Lett. **94**, 111109 (2009).
31. Y. C. Shen, G. O. Mueller, S. Watanabe, N. F. Gardner, A. Munkholm, and M. R. Krames, "Auger recombination in InGaN measured by photoluminescence," Appl. Phys. Lett. **91**, 141101 (2007).
32. X. Meng, L. Wang, Z. Hao, Y. Luo, C. Sun, Y. Han, B. Xiong, J. Wang, and H. Li, "Study on efficiency droop in InGaN/GaN light-emitting diodes based on differential carrier lifetime analysis," Appl. Phys. Lett. **108**, 013501 (2016).
33. B.-C. Lin, K.-J. Chen, C.-H. Wang, C.-H. Chiu, Y.-P. Lan, C.-C. Lin, P.-T. Lee, M.-H. Shih, Y.-K. Kuo, and H.-C. Kuo, "Hole injection and electron overflow improvement in InGaN/GaN light-emitting diodes by a tapered AlGaN electron blocking layer," Opt. Express **22**, 463-469 (2014).
34. E. F. Schubert, T. Gessmann, and J. K. Kim, "Light emitting diodes," in *Kirk-Othmer Encyclopedia of Chemical Technology*, 2nd ed. (John Wiley & Sons, NY, USA. 2005).
35. A. David and M. J. Grundmann, "Droop in InGaN light-emitting diodes: A differential carrier lifetime analysis," Appl. Phys. Lett. **96**, 103504 (2010).
36. J. Piprek, "Efficiency droop in nitride-based light-emitting diodes," Phys. Status Solidi A **207**, 2217-2225 (2010).
37. C.-K. Sun, S. Keller, G. Wang, M. Minsky, J. E. Bowers, and S. P. DenBaars, "Radiative recombination lifetime measurements of InGaN single quantum well," Appl. Phys. Lett. **69**, 1936-1938 (1996).
38. F. Römer and B. Witzigmann, "Effect of Auger recombination and leakage on the droop in InGaN/GaN quantum well LEDs," Opt. Express **22**, A1440-A1452 (2014).
39. H. Zhao, G. Liu, J. Zhang, R. A. Arif, and N. Tansu, "Analysis of internal quantum efficiency and current injection efficiency in III-nitride light-emitting diodes," J. Disp. Technol. **9**, 212-225 (2013).
40. M. Deppner, F. Römer, and B. Witzigmann, "Auger carrier leakage in III-nitride quantum-well light emitting diodes," Phys. Status Solidi Rapid Res. Lett. **6**, 418-420 (2012).
41. J. Hader, J. V. Moloney, B. Pasenow, S. W. Koch, M. Sabathil, N. Linder, and S. Lutgen, "On the importance of radiative and Auger losses in GaN-based quantum wells," Appl. Phys. Lett. **92**, 261103 (2008).
42. C. H. Wang, C. C. Ke, C. Y. Lee, S. P. Chang, W. T. Chang, J. C. Li, Z. Y. Li, H. C. Yang, H. C. Kuo, T. C. Lu, and S. C. Wang, "Hole injection and efficiency droop improvement in InGaN/GaN light-emitting diodes by band-engineered electron blocking layer," Appl. Phys. Lett. **97**, 261103 (2010).
43. R. M. Perks, A. Porch, D. V. Morgan, and J. Kettle, "Theoretical and experimental analysis of current spreading in AlGaInP light emitting diodes," J. Appl. Phys. **100**, 083109 (2006).
44. B. Laikhtman, A. Gourevitch, D. Donetsky, D. Westerfeld, and G. Belenky, "Current spread and overheating of high power laser bars," J. Appl. Phys. **95**, 3880-3889 (2004).